Importin-β targets HURP to kinetochore-fibers in coordination with Ran-GTP in human mitotic cells

Kenta Tsuchiya[1], Hisato Hayashi[1], Momoko Nishina[1], Masako Okumura[1], Masato T. Kanemaki[2,3], Gohta Goshima[1], Tomomi Kiyomitsu[1,2]*

[1] Division of Biological Science, Graduate School of Science, Nagoya University, Chikusa-ku, Nagoya 464-8602, Japan.

[2] Precursory Research for Embryonic Science and Technology (PRESTO) Program, Japan Science and Technology Agency, 4-1-8 Honcho Kawaguchi, Saitama 332-0012, Japan.

[3] Molecular Cell Engineering Laboratory, National Institute of Genetics, Research Organization of Information and Systems (ROIS), and Department of Genetics, SOKENDAI (The Graduate University of Advanced Studies), Yata 1111, Mishima, Shizuoka 411-8540, Japan.

* Corresponding author:
E-mail: kiyomitsu@bio.nagoya-u.ac.jp
Phone & Fax: +81-52-788-6174
Characters: 29,170 characters

Abstract

During spindle assembly, microtubules are spatially organized by the chromosome-derived Ran-GTP gradient. Previous work demonstrated that Ran-GTP releases spindle assembly factors such as HURP from inhibitory importins to assemble microtubules near chromosomes. However, the significance and mechanisms of Ran-mediated spindle assembly remains poorly understood, especially in somatic cells. Here, we systematically depleted RCC1 (Ran-GEF), RanGAP1, and importin-β in human cells using auxin-inducible degron technology. We demonstrate that depletion of RCC1, but not RanGAP1, causes short metaphase spindles that lack HURP on kinetochore-fibers (k-fibers). Surprisingly, we find that importin-β co-localizes with HURP to k-fibers, where it acts as an active, not inhibitory, regulator for HURP. HURP and importin-β are mutually dependent for their k-fiber localization and coordinately regulated by Ran-GTP. In addition, importin-β mutants lacking Ran-GTP binding fail to accumulate on k-fibers. Together, we propose a model in which, in the presence of microtubules, importin-β still interacts with HURP following Ran-GTP binding and further promotes HURP's microtubule association to stabilize k-fibers.

(160 words)

42 **Introduction**

43 The spindle is a universal microtubule-based macromolecular structure that plays
44 crucial roles for accurate cell division in eukaryotes (McIntosh and Hays, 2016). The
45 spatial organization of microtubules and microtubule-associated proteins is crucial for
46 the proper assembly and function of the spindle in both mitosis and meiosis (Bennabi et
47 al., 2016; Heald and Khodjakov, 2015). During animal mitosis, both chromosome- and
48 centrosome-derived signals organize the mitotic spindle structure by spatially regulating
49 microtubule nucleation, polymerization/depolymerization, transport, sliding, and cross-
50 linking (Goshima and Scholey, 2010; Petry, 2016; Walczak and Heald, 2008). During
51 female meiosis, chromosome-derived signals play particularly dominant roles in spindle
52 assembly as centrosomes are absent (Beaven et al., 2017; Bennabi et al., 2016;
53 Mogessie et al., 2018).

54 Chromosome-derived signals consist of two distinct pathways - the Ran-GTP
55 gradient and chromosome passenger complex (CPC)-based signals (Zierhut and
56 Funabiki, 2015). Pioneering work using meiotic *Xenopus* egg extracts established a
57 model in which a chromosome-derived Ran-GTP gradient promotes spindle assembly
58 by activating spindle assembly factors (SAFs) such as NuMA and TPX2 by releasing
59 them from inhibitory importin proteins in the vicinity of chromosomes (Fig.1A) (Kalab
60 and Heald, 2008; Nachury et al., 2001; Wiese et al., 2001). At present, several
61 microtubule-binding proteins, such as HURP (Forbes et al., 2015; Sillje et al., 2006),
62 have been identified as spindle assembly factors that promote spindle assembly
63 downstream of Ran-GTP gradient (Forbes et al., 2015). In parallel, chromatin-bound
64 CPC promotes microtubule polymerization around chromosomes by locally inhibiting

65 microtubule-destabilizing factors such as MCAK and Op18 (Kelly et al., 2007; Maresca
66 et al., 2009; Sampath et al., 2004).

67 The Ran-GTP gradient is generated by two spatially-separated opposing
68 enzymes. Regulator of chromosome condensation 1 (RCC1), is a guanine nucleotide
69 exchange factor (GEF) for Ran (Bischoff and Ponstingl, 1991) and localizes to
70 chromosomes to convert the small GTPase Ran from its GDP- to GTP-bound form. In
71 contrast, RanGAP1, a GTPase-activating protein (GAP) for Ran, predominantly
72 localizes to the cytoplasm to promote Ran's intrinsic GTPase activity (Bischoff et al.,
73 1994) (Fig. 1A). The Ran-GTP gradient has been best characterized in meiotic *Xenopus*
74 egg extracts, but is also found in other meiotic and mitotic cell types (Dumont et al.,
75 2007; Kalab et al., 2006; Moutinho-Pereira et al., 2013). In addition to a role in spindle
76 assembly, we previously demonstrated that the Ran-GTP gradient promotes spindle
77 positioning by controlling the spatial organization of cortical complexes in somatic
78 human cells (Kiyomitsu and Cheeseman, 2012; Kiyomitsu and Cheeseman, 2013).
79 Although the Ran-GTP gradient is conserved and critical for meiotic spindle assembly
80 (Dumont et al., 2007; Holubcova et al., 2015), its significance for mitotic spindle
81 assembly has been debated and appears to vary across cell types (Furuta et al., 2016;
82 Hasegawa et al., 2013; Moutinho-Pereira et al., 2013).

83 To understand the significance and mechanisms of Ran-mediated spindle
84 assembly in human mitotic cells, we sought to systematically deplete and visualize
85 endogenous Ran-associated proteins in living cells by combining auxin-inducible degron
86 (AID) technology and CRISPR/Cas9-mediated genome editing (Natsume et al., 2016).
87 We found that degradation of RCC1 causes short mitotic spindle and disrupts the

88 spatial localization of HURP in human cells. Unexpectedly, we found that importin-β
89 depletion caused mitotic phenotypes similar to RCC1 depletion, but not RanGAP1
90 depletion, which is opposite to what is predicted based on prevailing models (Fig. 1A).
91 Importantly, we demonstrate that importin-β co-localizes with HURP to k-fibers
92 downstream of RCC1 and that importin-β enriches HURP on k-fibers in coordination
93 with Ran-GTP gradient. Based on our findings, we propose a revised model that, in the
94 presence of microtubules, importin-β is still able to interact with HURP following Ran-
95 GTP-binding and positively regulates HURP's k-fiber localization in coordination with
96 Ran-GTP to promote functional k-fiber assembly.
97

98 **Results**

99 **Auxin-inducible degradation of RCC1 causes short spindle in human cells**

100 To understand the molecular mechanisms of Ran-GTP-dependent spindle assembly in
101 mitotic human cells, we sought to systematically deplete Ran-associated proteins using
102 auxin-inducible degron (AID) technology (Fig. 1A, B) (Natsume et al., 2016). We first
103 targeted RCC1, a Ran-GEF, which should deplete the GTP-bound form of Ran. We
104 introduced a C-terminal mAID-mClover (mAC) tag into both alleles of the RCC1
105 genomic locus (Fig. 1C and Fig. S1A) in parental tet-OsTIR1 HCT116 cells that
106 conditionally express OsTIR1 following the addition of doxycycline (Dox) (Fig.1B)
107 (Natsume et al., 2016). To visualize NuMA, a spindle assembly factors regulated by
108 Ran (Chang et al., 2017; Nachury et al., 2001; Wiese et al., 2001), we further integrated
109 mCherry into both alleles of the NuMA genomic locus (Fig. 1C and S1B). This double
110 knock-in cell line grew normally, and both RCC1-mAC and NuMA-mCherry displayed
111 their expected localization patterns (Fig. 1D, E). This suggests that these fusion
112 constructs did not affect the functions of endogenous RCC1 and NuMA.

113 To analyze the functions of RCC1, we performed time-lapse imaging of RCC1-
114 depleted cells following treatment with Dox and auxin (IAA). After 18-24 hrs, the
115 fluorescence intensity of RCC1-mAC was reduced to undetectable levels (Fig. 1D-F),
116 although some populations of cells still displayed RCC1-mAC signals possibly due to
117 heterogeneous induction of OsTIR1 (Fig. 1F, 2nd panels). RCC1-depleted cells
118 progressed through mitosis, but nuclear shape was severely impaired following mitotic
119 exit (Fig. 1F, t=1:00). This is consistent with the phenotypes observed in RCC1-depleted
120 chicken DT40 cells (Furuta et al., 2016). NuMA did not localize to these abnormal nuclei

121 (Fig. 1F, t=1:00), whereas NuMA still localized to the nucleus prior to mitosis even in the
122 absence of RCC1 (Fig. 1F, t= - 0:10). This suggests that NuMA is maintained in the
123 nucleus once imported. Importantly, metaphase spindle length became shorter in
124 RCC1-depleted cells (Fig. 1D, G). In addition, mitotic duration from nuclear envelope
125 breakdown (NEBD) to anaphase onset was slightly but significantly delayed (Fig. 1F, H).
126 However, the spindle localization of NuMA was virtually unaffected following RCC1
127 depletion (Fig. 1D-F). These results suggest that RCC1 is required for proper spindle
128 assembly and mitotic progression in human HCT116 cells, probably by activating the
129 functions of spindle assembly factors distinct from NuMA.

130

131 **RanGAP1 is dispensable for mitotic spindle assembly**

132 To analyze the functional contributions of the Ran-GTP gradient during mitosis, we next
133 sought to increase Ran-GTP level by depleting RanGAP1. Endogenously tagged
134 RanGAP1 (RanGAP1-mAC) localized to the cytoplasm and was excluded from
135 chromosomes (Fig. 2A-B, S1C-D), but was also weakly detectable at kinetochores in
136 metaphase, consistent with prior work (Joseph et al., 2002). However, degradation of
137 RanGAP1 did not cause a clear phenotype during mitosis (Fig. 2B-D, Fig. S1E-F): the
138 bipolar spindle assembled normally, and metaphase spindle length and mitotic duration
139 in RanGAP1-depleted cells were almost identical to those in control cells. These results
140 suggest that RanGAP1-mediated hydrolysis of Ran-GTP is dispensable for mitotic
141 spindle assembly in HCT116 cells.

142

143 **Degradation of importin-β causes mitotic phenotypes similar to RCC1, but not**
144 **RanGAP1 depletion**

145 In the current model, Ran-GTP activates spindle assembly factors by releasing them
146 from inhibitory importins in the vicinity of chromosomes (Fig. 1A). Based on this model,
147 depletion of importin-β would liberate spindle assembly factors throughout the cell
148 resulting in mitotic phenotypes similar to Ran-GAP1 depletion. To test this, we next
149 depleted endogenous importin-β by fusing it with mAID-mClover (mAC) (Fig. 2E, F and
150 Fig. S2A-B). Unexpectedly, we found that endogenous importin-β-mAC accumulated at
151 the chromosome-proximal region of bundled kinetochore-microtubules (k-fibers) in living
152 cells (Fig. 2F top, S2C). This contrasts with a previous study that found importin-β
153 localizes to spindle poles in pre-extracted fixed cells (Ciciarello et al., 2004). The k-fiber
154 localization of importin-β was not an artifact of mAC tagging, as it was observed after
155 immunostaining of endogenous importin-β without tags (Fig. S2D). Importantly,
156 importin-β depletion resulted in a defective spindle structure characterized by short
157 mitotic spindles and delayed mitotic progression (Fig. 2G-J), although NuMA's
158 localization was almost normal (Fig. 2F, H). This phenotype is similar to RCC1 depletion,
159 but not RanGAP1 depletion. These results suggest that, in contrast to prevailing models
160 (Fig. 1A), importin-β promotes spindle assembly, but does not inhibit this process.

161

162 **RCC1 and importin-β are required for HURP localization to k-fibers**

163 The phenotypic similarity between importin-β and RCC1 depletions was not readily
164 explainable by the current model in which Ran activates spindle assembly factors by
165 releasing inhibitory importins (Fig. 1A). Rather, it could be interpreted that importin-β

166 positively regulates spindle assembly factors downstream of RCC1 to promote spindle
167 assembly. To test this possibility, we next analyzed the localization of importin-β and
168 known spindle assembly factors including NuMA, TPX2 (Gruss et al., 2001), and HURP
169 (Sillje et al., 2006). Strikingly, RCC1 depletion abolished k-fiber accumulation of both
170 importin-β (Fig. 3A, Fig. S2E) and HURP(Fig. 3B, Fig. S2F). HURP localized diffusely
171 in the cytoplasm with weak accumulation at spindle poles in RCC1-depleted cells (Fig.
172 3B). In contrast, the spindle localization of NuMA (Fig. 1D) and TPX2 was virtually
173 unaffected in RCC1-depleted cells (Fig. 3C and S2G).

174 We next analyzed HURP localization in importin-β-depleted cells. In control cells,
175 importin-β co-localized with SNAP-tagged endogenous HURP (HURP-SNAP) to k-fibers
176 (Fig. 3D top, S2H). However, importin-β depletion abolished the k-fiber localization of
177 HURP, resulting in strong accumulation of HURP at spindle poles of the short spindle
178 (Fig. 3D bottom, Fig. S2I). These results suggest that HURP is a key downstream target
179 of importin-β in human HCT116 cells.

180

181 **HURP is required to target importin-β to k-fibers and control proper metaphase**
182 **spindle length**

183 Previous work demonstrated that importin-β directly interacts with HURP (Sillje et al.,
184 2006). However, it was assumed that importin-β dissociates from HURP following the
185 binding of Ran-GTP to importin-β (Fig. 1A) (Sillje et al., 2006). To understand the
186 relationship between importin-β and HURP for their k-fiber localization and function, we
187 next targeted endogenous HURP by introducing a mAID-mClover-3xFLAG (mACF) tag
188 (Fig. 4A, Fig. S3A). In control cells, HURP-mACF co-localized with endogenous

189 mCherry-tagged importin-β (importin-β-mCh) on k-fibers (Fig. 4B top, Fig. S3B).
190 However, HURP depletion resulted in diminished importin-β to k-fibers (Fig. 4B, bottom,
191 4C) and reduced mitotic spindle length (Fig. 4D) as observed for importin-β depleted
192 cells (Fig. 2I). These results suggest that HURP localizes to k-fiber along with importin-β,
193 likely by maintaining the interaction with importin-β.

194

195 **Ran-GTP promotes spindle microtubule enrichment of HURP and importin-β.**

196 In contrast to prior expectations, our results suggest that importin-β acts positively to
197 target HURP to k-fibers following Ran-GTP binding instead of dissociating from HURP.
198 To probe this model, we next analyzed the behaviors of importin-β and HURP in
199 RanGAP1-depleted cells in which Ran-GTP levels are expected to be increased.
200 Intriguingly, following the depletion of RanGAP1, both importin-β and HURP localized to
201 k-fibers, but additionally accumulated on spindle microtubules with increased intensities
202 (Fig. 5A-B, Fig. S1D). This suggests that importin-β and HURP behave together and
203 interact with microtubules more stably in response to Ran-GTP.

204

205 **Ran-GTP binding to importin-β is required for k-fiber localization of importin-β**

206 Ran-GTP directly binds to importin-β, resulting in cargo release from importin-β (Fig.1A)
207 (Lee et al., 2005; Zachariae and Grubmuller, 2008). However, our results indicate that
208 importin-β still interacts with HURP following Ran-GTP binding and localizes to k-fibers
209 together with HURP and Ran-GTP. To test this model, we next sought to analyze
210 whether Ran-GTP localizes to k-fibers. To visualize Ran-GTP, we expressed a

211 constitutively active mutant of Ran, RanQ69L, that is unable to hydrolyze bound GTP
212 (Bischoff et al., 1994) and thus expected to be as GTP-bond form. Consistent with our
213 model, ectopically-expressed mCherry-tagged RanQ69L was detected on k-fibers (25 %,
214 n=68, Fig. 5C and Fig. S4A) in HEK293 cells. In contrast, a dominant negative mutant
215 that is unable to bind to GTP, mCh-RanT24N, predominantly localized to chromosomes
216 (100%, n=30) (Fig. 5C) (Kiyomitsu and Cheeseman, 2012) and was never detected on
217 k-fibers.

218 We next analyzed whether Ran-GTP binding to importin-β is required for the k-
219 fiber localization of importin-β. For this, we analyzed the localization of importin-β ΔN10
220 and ΔN70 mutants that are compromised or completely unable to bind Ran-GTP,
221 respectively (Chi et al., 1997; Kutay et al., 1997), but are still able to interact with HURP
222 (Song and Rape, 2010). Transiently expressed mCherry-tagged wild type (WT)
223 importin-β displayed k-fiber-like localization in ~40 % of HEK293 cells (Fig. 5D, n=62).
224 In contrast, both importin-β ΔN10 and ΔN70 mutants failed to localize to k-fibers, but
225 instead accumulated on spindle microtubules or spindle poles (Fig. 5D), probably by
226 binding to its other cargos. These results support our model that importin-β localizes to
227 k-fibers by binding to Ran-GTP.
228

229 **Discussion**

230 **Importin-β positively regulates HURP's k-fiber accumulation.**

231 Here, we found that importin-β co-localizes with HURP to k-fibers (Fig. 2F, 3D, 4B, S2D),
232 and positively regulates metaphase spindle length and HURP's k-fiber accumulation
233 (Fig. 2I, 3D) in response to the Ran-GTP gradient (Fig. 3A-B, 5A-B, D). Based on these
234 findings, we propose a revised model in which Ran-GTP binding to HURP-importin-β
235 complexes leads to different outcomes in response to the presence or absence of
236 microtubules (Fig. 6).

237 Upon Ran-GTP binding, importin-β changes its conformation (Lee et al., 2005),
238 which leads to dissociation of importin-β from HURP in the cytoplasm (Sillje et al., 2006;
239 Song and Rape, 2010) (Fig. 6, Classical model). However, given that HURP's importin-
240 β binding region is located within the second microtubule-binding domain (MBD2) of
241 HURP (Song and Rape, 2010), we hypothesize that, in the presence of microtubules,
242 HURP captures microtubules through its MBD2 domain without releasing Ran-GTP
243 bound importin-β (Fig. 6, New model-I). Since the microtubule-binding domain (MBD1)
244 of HURP constitutively interacts with microtubules even in the presence of importin-β
245 (Song et al., 2014), a HURP-importin-β-Ran-GTP ternary complex may bundle k-fibers
246 by linking different microtubules using two microtubule-binding domains (MBD1 and 2)
247 of HURP (Fig. 6, New model-I). This model is consistent with previous in vitro studies
248 reported by Sillje et al. (Sillje et al., 2006) in which purified microtubules were mixed
249 with recombinant HURP, importin-β and RanQ69L. Whereas importin-β addition to
250 HURP and microtubules largely suppressed HURP's microtubule bundling activity,
251 simultaneous addition of importin-β and RanQ69L resulted in HURP that still displayed

252 mild microtubule bundling (see Figure 7b in (Sillje et al., 2006)), suggesting that Ran-
253 GTP suppresses importin-β's inhibitory activity in the presence of microtubules. The
254 Ran-GTP dependent activation of HURP-importin-β complexes may be suitable for
255 bundling short microtubules nucleated around kinetochores to form stable k-fibers
256 (Sikirzhytski et al., 2018).

257

258 **Importin-β has dual functions in response to the Ran-GTP gradient to amplify**
259 **HURP's k-fiber accumulation**

260 Although HURP has microtubule-binding activities, we demonstrate that HURP itself is
261 unable to localize to k-fibers in the absence of importin-β, and instead accumulates on
262 spindle microtubules around spindle poles (Fig. 3D). This indicates that importin-β
263 functions not only to enrich HURP on k-fibers, but also to exclude HURP from spindle
264 microtubules around the spindle poles. We propose that importin-β increases the
265 microtubule-binding affinity of HURP by exposing its MBD2 domain following Ran-GTP
266 binding around chromosomes (Fig. 6, New model-I), and decreases HURP's
267 microtubule binding activity by masking MBD2 around the spindle poles (Fig. 6, New
268 model-II). Thus, importin-β can act either positively or negatively in response to the
269 Ran-GTP gradient to synergistically enrich HURP on k-fibers near chromosomes.

270

271 **K-fiber accumulation of HURP-importin-β complexes is required for proper**
272 **metaphase spindle formation**

273 We found that degradation of either RCC1, importin-β, or HURP, but not RanGAP1,
274 caused short metaphase spindles in human HCT116 cells (Fig. 1G, 2C, 2I, S2I, 4D).
275 Because HURP is required for the stabilization of k-fibers (Sillje et al., 2006) and the
276 generation or maintenance of spindle microtubules (Uehara and Goshima, 2010), loss
277 of k-fiber accumulation of HURP would lead to destabilization of k-fibers and/or spindle
278 microtubules resulting in short metaphase spindles. In contrast, NuMA and TPX2
279 accumulate around spindle poles even in the absence of RCC1 (Fig. 1D, 3C). Given the
280 severe defects in bipolar spindle assembly following NuMA or TPX2 depletion (Garrett
281 et al., 2002; Hueschen et al., 2017; Okumura et al., 2018), NuMA and TPX2 would be
282 able to function independently of Ran-GTP in HCT116 cells. In fact, co-depletion of
283 RCC1 and NuMA caused severe mitotic phenotypes (T.K. unpublished observation).
284 Other Ran-GTP independent mechanisms may exist to liberate these spindle assembly
285 factors from importins in mitotic cells. In addition, other mechanisms such as CPC-
286 dependent spindle assembly (Kelly et al., 2007; Maresca et al., 2009; Sampath et al.,
287 2004) and TACC3/chTOG/clathrin complex-mediated k-fiber stabilization (Booth et al.,
288 2011) may play dominant roles to assemble a functional spindle in mitotic cells. In
289 contrast to mitosis, Ran pathway plays critical roles for spindle assembly in female
290 meiosis (Dumont et al., 2007; Holubcova et al., 2015). It will be interesting to test
291 whether our model (Fig. 6) is conserved in meiosis.

292

293

Acknowledgments

We thank I. M. Cheeseman for critical reading of the manuscript, R. Inaba, and K. Murase for technical assistance. This work was supported by grants from PRESTO program (JPMJPR13A3) of the Japan Science and Technology agency (JST) for T.K, a Career Development Award of the Human Frontier Science Program (CDA00057/2014-C) for T.K., KAKENHI (16K14721 and 17H05002 for T.K, 17H01431 for G.G.) of the Japan Society for Promotion of Science (JSPS), Collaborative Research Program (2014-B, 2015-A1, 2016-A1 for T.K and M.K) of the National Institute of Genetics (NIG), and the Naito Foundation for T.K.

Author contributions

Conceptualization, T.K. ; Investigation, K.T., H.H., M.N., M.O, and T.K. ; Formal analysis, K.T., and T.K. ; Methodology, T.K. and M.K. ; Writing, T.K. and G.G. ; Supervision, T.K. and G.G. ; Funding Acquisition, T.K., M.K. and G.G.

Declaration of interests

The authors declare no competing interests.

Materials and methods

- Plasmid Construction

  Plasmids for CRISPR/Cas9-mediated genome editing and auxin-inducible degron were constructed according to the protocol described in Natsume et al., (Natsume et al., 2016) and Okumura et al., (Okumura et al., 2018). To construct donor plasmids containing homology arms for RCC1 (~500-bp homology arms), RanGAP1 (~500-bp arms), importin-β (~500-bp homology arms), HURP (~200-bp homology arms), and TPX2 (~200-bp homology arms), gene synthesis services from Eurofins Genomics K.K. (Tokyo, Japan) or Genewiz (South Plainsfield, NJ) were used for RCC1 and others, respectively. To express mCherry-tagged Ran or importin-β mutants, the cDNA sequences were inserted into plasmid pIC194 (#44433, Addgene)(Kiyomitsu and Cheeseman, 2012), which contains a 61 amino acid linker between mCherry and the coding sequence. Plasmids and sgRNA sequences used in this study are listed in Supplementary Tables S1 and S2, and will be deposited to Addgene.

- Cell Culture, Cell Line Generation and Antibodies

  HCT116 cells and Flip-in TRex 293 cells were cultured as described previously (Kiyomitsu et al., 2011; Okumura et al., 2018). Knock-in cell lines for HCT116 cells or Flip-In TRex 293 cells were generated according to the procedures described in Okumura et al., (Okumura et al., 2018) or Kiyomitsu et al., (Kiyomitsu et al., 2011), respectively. To activate the auxin-inducible degradation, cells were treated with 2 μg/mL Dox and 500 μM indoleacetic acid (IAA) for 20–24 h. Cells with undetectable mClover signals were analyzed. To expresss mCherry-tagged Ran mutants in Fig. 5C, cells were incubated with 1 μg/mL tetracycline (MP biomedicals) for >18 h. The cell lines and primers used in this study are listed in Tables S1 and S3, respectively.

  Antibodies against tubulin (DM1A, Sigma-Aldrich, 1:2,000), NuMA (Abcam, 1:1,000), RCC1 (Cell Signaling Technology, D15H6, Rabbit mAb, 1:100), RanGAP1 (Santa Cruz Biotechnology, H-180, 1:200), importin-β (GeneTex, 3E9 Mouse mAb, 1:100), and HURP (E. Nigg laboratory, 1 : 200) were used for western blotting. For RCC1 immunoblots, the membrane was incubated with the anti-RCC1 antibody overnight at 4 °C.

- Microscope System

  Imaging was performed using spinning-disc confocal microscopy with a 60× 1.40 numerical aperture objective lens (Plan Apo λ, Nikon, Tokyo, Japan). A CSU-W1 confocal unit (Yokogawa Electric Corporation, Tokyo, Japan) with three lasers (488, 561, and 640 nm, Coherent, Santa Clara, CA) and an ORCA-Flash4.0 digital CMOS camera (Hamamatsu Photonics, Hamamatsu City, Japan) were attached to an ECLIPSE Ti-E inverted microscope (Nikon) with a perfect focus system. DNA images were obtained using SOLA LED light engine (Lumencor, Beaverton, OR) and appropriate filters. A stage-top incubator (Tokai Hit, Fujinomiya, Japan) was used to maintain the same conditions used for cell culture (37 °C and 5% CO_2).

- Immunofluorescence and Live Cell Imaging

  For immunofluorescence in Figure S2D, HURP-mACF cells were fixed with PBS

containing 3% paraformaldehyde and 2% sucrose for 10 min at room temperature. Fixed cells were permeabilized with 0.5% Triton X-100™ for 5 min on ice, and pretreated with PBS containing 1% BSA for 10 min at room temperature after washing with PBS. Importin-β was visualized using the anti-importin-β antibody (1:500). Images of multiple z-sections were acquired by spinning-disc confocal microscopy using 0.5-μm spacing and camera binning 2. Maximally projected images from 3 z-sections were shown.

For time-lapse imaging in Fig. 1E-F, S1E-F and Fig. 2G-H, cells were cultured on glass-bottomed dishes (CELLview™, #627870, Greiner Bio-One, Kremsmünster, Austria) and maintained in a stage-top incubator (Tokai Hit) to maintain the same conditions used for cell culture (37 °C and 5% CO_2). Two z-section images using 1.0-μm spacing were acquired with camera binning 2 and maximally projected z-stack images were shown. In other live cell imaging, three to five z-section images using 0.5-μm spacing were acquired and single z-section images were shown, unless otherwise specified. Microtubules was stained with 50 nM SiR-tubulin (Spirochrome) for >1 h prior to image acquisition. DNA was stained 50 ng/mL Hoechst® 33342 (Sigma-Aldrich) for > 1 h before observation. To visualize SNAP-tagged HURP in Fig. 3D, cells were incubated with 0.1 μM TMR-STAR (New England BioLabs) for > 2 h, and those chemical probes were removed before observation. To optimize image brightness, same linear adjustments were applied using Fiji and Photoshop.

- Statistical Analysis

To determine the significance of differences between the mean values obtained for two experimental conditions, Welch's *t*-tests (Prism 6; GraphPad Software, La Jolla, CA) or a Z-test for proportions (Allto Consulting, Leeds, UK) were used as indicated in the figure legends.

388 **Table S1: Cell lines used in this study.**

No.	Name	Description	Clone No.	Plasmids used	Parental cell	Reference
1	HCT116 tet-OsTIR1	AAVS1::PTRE3G OsTIR1 (Puro)		pAAVS1 T2 and MK243 (Addgene#72835)		(Natsume et al., 2016)
2	RCC1-mAC	AAVS1::PTRE3G OsTIR1 (Puro), RCC1:: RCC1-mAID-mClover (Neo)	1	pTK361+ pHH45	1	This study
3	RCC1-mAC + NuMA-mCh	AAVS1::PTRE3G OsTIR1 (Puro), RCC1:: RCC1-mAID-mClover (Neo), NuMA1:: NuMA-mCh (Hygro)	1	pTK372+ pTK435	2	This study
4	RanGAP1-mAC	AAVS1::PTRE3G OsTIR1 (Puro), RanGAP1:: RanGAP1-mAID-mClover (Neo)	9	pHH49 + pHH51	1	This study
5	RanGAP1-mAC + NuMA-mCh	AAVS1::PTRE3G OsTIR1 (Puro), RanGAP1:: RanGAP1-mAID-mClover (Neo), NuMA1:: NuMA-mCh (Hygro)	5	pTK372+ pTK435	4	This study
6	importin-β-mAC	AAVS1::PTRE3G OsTIR1 (Puro), importin-β:: importin-β-mAID-mClover (Neo)	7	pHH50 + pHH57	1	This study
7	importin-β-mAC + NuMA-mCh	AAVS1::PTRE3G OsTIR1 (Puro), importin-β:: importin-β-mAID-mClover (Neo), NuMA1:: NuMA-mCh (Hygro)	1	pTK372+ pTK435	6	This study
8	RCC1-mAC + importin-β-mCh	AAVS1::PTRE3G OsTIR1 (Puro), RCC1:: RCC1-mAID-mClover (Neo), NuMA1:: NuMA-mCh (Hygro)	6	pHH50 +pTK481	2	This study
9	RCC1-mAC + HURP-mCh	AAVS1::PTRE3G OsTIR1 (Puro), RCC1:: RCC1-mAID-mClover (Neo), HURP:: HURP-mCh (Hygro)	8	pTK532+ pTK541	2	This study
10	RCC1-mAC + TPX2-mCh	AAVS1::PTRE3G OsTIR1 (Puro), RCC1:: RCC1-mAID-mClover (Neo), TPX2:: TPX2-mCh (Hygro)	1	pTK527+ pTK502	2	This study
11	RanGAP1-mAC + HURP-mCh	AAVS1::PTRE3G OsTIR1 (Puro), RanGAP1:: RanGAP1-mAID-mClover (Neo), HURP:: HURP-mCh (Hygro)	5	pTK532+ pTK541	4	This study
12	RanGAP1-mAC + importin-β-mCh	AAVS1::PTRE3G OsTIR1 (Puro), RanGAP1:: RanGAP1-mAID-mClover (Neo), importin-β:: importin-β-mCh (Hygro)	12	pHH50 +pTK481	4	This study
13	importin-β-mAC + HURP-SNAP	AAVS1::PTRE3G OsTIR1 (Puro), importin-β:: importin-β-mAID-mClover (Neo), HURP:: HURP-SNAP (Hygro)	3	pTK532+ pTK589	6	This study
14	HURP-mACF	AAVS1::PTRE3G OsTIR1 (Puro), HURP:: HURP-mAID-mClover-3FLAG (Neo)	13	pTK532+ pTK596	1	This study
15	HURP-mACF + importin-β-mCh	AAVS1::PTRE3G OsTIR1 (Puro), HURP:: HURP-mAID-mClover-3FLAG (Neo), importin-β:: importin-β-mCh (Hygro)	14	pHH50 +pTK481	14	This study
16	HEK293 Flip-In TRex					(Kiyomitsu et al., 2011)
17	HEK293 Flip-In TRex + mCh-RanT24N	Flip-In:: mCh-RanT24N (Hygro)	1	pTK285+ pOG44	16	This study
18	HEK293 Flip-In TRex + mCh-RanQ69L	Flip-In:: mCh-RanQ69L (Hygro)	1	pTK286+ pOG44	16	This study

389 **Table S2: sgRNA sequences for CRISPR/Cas9-mediated genome editing**

Gene locus	sgRNA (5'-3')	PAM	Plasmid Name
NuMA1 (C-terminus)	gtggggccactcactggtac	tgg	pTK372 (Okumura et al., 2018)
RCC1 (C-terminus)	gactgtatgctggcccccgc	tgg	pTK361
RanGAP1 (C-terminus)	tctgctgcagacgctgtaca	agg	pHH49
importin-β (C-terminus)	agttcgagccgccgcccgaa	agg	pHH50
HURP	caaaattctcctggttgtag	agg	pTK532
TPX2	tgcggataccgcccggcaat	ggg	pTK527

390

391 **Table S3: PCR primers to confirm gene editing**

Gene	Primer sequence	Primer name	Figures
RCC1	gaatgccattccaggcag	oHH88	Figure S1A
RCC1	ttctgcacgttcctctgg	oHH89	Figure S1A
NUMA1	gagcctcaaagaaggccc	oTK542	Figure S1B, S1D, S2B
NUMA1	agcaggaaccagggcctac	oTK566	Figure S1B, S1D, S2B
RanGAP1	gctgccgcaggaccagggcttggtg	oHH93	Figure S1C
RanGAP1	attccctggcctatgtctgctggaa	oHH94	Figure S1C
HURP	ctcttgatggatactttactg	oTK749	Figure S1D, S2F, S2H, S3A
HURP	cccttgagaaagagtatatcta	oTK750	Figure S1D, S2F, S2H, S3A
importin-β	ggagtaaggagttttgagagtatcg	oHH97	Figure S1D, S2A, S2E, S3B
importin-β	aaatcttctctagagctaggcaacg	oHH98	Figure S1D, S2A, S2E, S3B
TPX2	tctgacatccctctcactg	oTK660	Figure S2G
TPX2	ggagtctaatcgagacattc	oTK661	Figure S2G

392

393

394 ## References
395

396 Beaven, R., R.N. Bastos, C. Spanos, P. Rome, C.F. Cullen, J. Rappsilber, R. Giet, G. Goshima, and H. Ohkura. 2017.
397 14-3-3 regulation of Ncd reveals a new mechanism for targeting proteins to the spindle in oocytes. *J Cell*
398 *Biol*. 216:3029-3039.
399 Bennabi, I., M.E. Terret, and M.H. Verlhac. 2016. Meiotic spindle assembly and chromosome segregation in
400 oocytes. *J Cell Biol*. 215:611-619.
401 Bischoff, F.R., C. Klebe, J. Kretschmer, A. Wittinghofer, and H. Ponstingl. 1994. RanGAP1 induces GTPase
402 activity of nuclear Ras-related Ran. *Proc Natl Acad Sci U S A*. 91:2587-2591.
403 Bischoff, F.R., and H. Ponstingl. 1991. Catalysis of guanine nucleotide exchange on Ran by the mitotic regulator
404 RCC1. *Nature*. 354:80-82.
405 Booth, D.G., F.E. Hood, I.A. Prior, and S.J. Royle. 2011. A TACC3/ch-TOG/clathrin complex stabilises kinetochore
406 fibres by inter-microtubule bridging. *EMBO J*. 30:906-919.
407 Chang, C.C., T.L. Huang, Y. Shimamoto, S.Y. Tsai, and K.C. Hsia. 2017. Regulation of mitotic spindle assembly
408 factor NuMA by Importin-beta. *J Cell Biol*. 216:3453-3462.
409 Chi, N.C., E.J. Adam, and S.A. Adam. 1997. Different binding domains for Ran-GTP and Ran-GDP/RanBP1 on
410 nuclear import factor p97. *J Biol Chem*. 272:6818-6822.
411 Ciciarello, M., R. Mangiacasale, C. Thibier, G. Guarguaglini, E. Marchetti, B. Di Fiore, and P. Lavia. 2004.
412 Importin beta is transported to spindle poles during mitosis and regulates Ran-dependent spindle assembly
413 factors in mammalian cells. *J Cell Sci*. 117:6511-6522.
414 Dumont, J., S. Petri, F. Pellegrin, M.E. Terret, M.T. Bohnsack, P. Rassinier, V. Georget, P. Kalab, O.J. Gruss, and
415 M.H. Verlhac. 2007. A centriole- and RanGTP-independent spindle assembly pathway in meiosis I of
416 vertebrate oocytes. *J Cell Biol*. 176:295-305.
417 Forbes, D.J., A. Travesa, M.S. Nord, and C. Bernis. 2015. Reprint of "Nuclear transport factors: global regulation of
418 mitosis". *Curr Opin Cell Biol*. 34:122-134.
419 Furuta, M., T. Hori, and T. Fukagawa. 2016. Chromatin binding of RCC1 during mitosis is important for its nuclear
420 localization in interphase. *Mol Biol Cell*. 27:371-381.
421 Garrett, S., K. Auer, D.A. Compton, and T.M. Kapoor. 2002. hTPX2 is required for normal spindle morphology and
422 centrosome integrity during vertebrate cell division. *Curr Biol*. 12:2055-2059.
423 Goshima, G., and J.M. Scholey. 2010. Control of mitotic spindle length. *Annu Rev Cell Dev Biol*. 26:21-57.
424 Gruss, O.J., R.E. Carazo-Salas, C.A. Schatz, G. Guarguaglini, J. Kast, M. Wilm, N. Le Bot, I. Vernos, E. Karsenti,
425 and I.W. Mattaj. 2001. Ran induces spindle assembly by reversing the inhibitory effect of importin alpha
426 on TPX2 activity. *Cell*. 104:83-93.
427 Hasegawa, K., S.J. Ryu, and P. Kalab. 2013. Chromosomal gain promotes formation of a steep RanGTP gradient
428 that drives mitosis in aneuploid cells. *J Cell Biol*. 200:151-161.
429 Heald, R., and A. Khodjakov. 2015. Thirty years of search and capture: The complex simplicity of mitotic spindle
430 assembly. *J Cell Biol*. 211:1103-1111.
431 Holubcova, Z., M. Blayney, K. Elder, and M. Schuh. 2015. Human oocytes. Error-prone chromosome-mediated
432 spindle assembly favors chromosome segregation defects in human oocytes. *Science*. 348:1143-1147.
433 Hueschen, C.L., S.J. Kenny, K. Xu, and S. Dumont. 2017. NuMA recruits dynein activity to microtubule minus-
434 ends at mitosis. *Elife*. 6.
435 Joseph, J., S.H. Tan, T.S. Karpova, J.G. McNally, and M. Dasso. 2002. SUMO-1 targets RanGAP1 to kinetochores
436 and mitotic spindles. *J Cell Biol*. 156:595-602.
437 Kalab, P., and R. Heald. 2008. The RanGTP gradient - a GPS for the mitotic spindle. *J Cell Sci*. 121:1577-1586.
438 Kalab, P., A. Pralle, E.Y. Isacoff, R. Heald, and K. Weis. 2006. Analysis of a RanGTP-regulated gradient in mitotic
439 somatic cells. *Nature*. 440:697-701.
440 Kelly, A.E., S.C. Sampath, T.A. Maniar, E.M. Woo, B.T. Chait, and H. Funabiki. 2007. Chromosomal enrichment
441 and activation of the aurora B pathway are coupled to spatially regulate spindle assembly. *Dev Cell*. 12:31-
442 43.
443 Kiyomitsu, T., and I.M. Cheeseman. 2012. Chromosome- and spindle-pole-derived signals generate an intrinsic
444 code for spindle position and orientation. *Nat Cell Biol*. 14:311-317.
445 Kiyomitsu, T., and I.M. Cheeseman. 2013. Cortical dynein and asymmetric membrane elongation coordinately
446 position the spindle in anaphase. *Cell*. 154:391-402.

447 Kiyomitsu, T., H. Murakami, and M. Yanagida. 2011. Protein interaction domain mapping of human kinetochore
448 protein Blinkin reveals a consensus motif for binding of spindle assembly checkpoint proteins Bub1 and
449 BubR1. *Mol Cell Biol*. 31:998-1011.
450 Kutay, U., E. Izaurralde, F.R. Bischoff, I.W. Mattaj, and D. Gorlich. 1997. Dominant-negative mutants of importin-
451 beta block multiple pathways of import and export through the nuclear pore complex. *EMBO J*. 16:1153-
452 1163.
453 Lee, S.J., Y. Matsuura, S.M. Liu, and M. Stewart. 2005. Structural basis for nuclear import complex dissociation by
454 RanGTP. *Nature*. 435:693-696.
455 Maresca, T.J., A.C. Groen, J.C. Gatlin, R. Ohi, T.J. Mitchison, and E.D. Salmon. 2009. Spindle assembly in the
456 absence of a RanGTP gradient requires localized CPC activity. *Curr Biol*. 19:1210-1215.
457 McIntosh, J.R., and T. Hays. 2016. A Brief History of Research on Mitotic Mechanisms. *Biology (Basel)*. 5.
458 Mogessie, B., K. Scheffler, and M. Schuh. 2018. Assembly and Positioning of the Oocyte Meiotic Spindle. *Annu*
459 *Rev Cell Dev Biol*. 34:381-403.
460 Moutinho-Pereira, S., N. Stuurman, O. Afonso, M. Hornsveld, P. Aguiar, G. Goshima, R.D. Vale, and H. Maiato.
461 2013. Genes involved in centrosome-independent mitotic spindle assembly in Drosophila S2 cells. *Proc*
462 *Natl Acad Sci U S A*. 110:19808-19813.
463 Nachury, M.V., T.J. Maresca, W.C. Salmon, C.M. Waterman-Storer, R. Heald, and K. Weis. 2001. Importin beta is
464 a mitotic target of the small GTPase Ran in spindle assembly. *Cell*. 104:95-106.
465 Natsume, T., T. Kiyomitsu, Y. Saga, and M.T. Kanemaki. 2016. Rapid Protein Depletion in Human Cells by Auxin-
466 Inducible Degron Tagging with Short Homology Donors. *Cell Rep*. 15:210-218.
467 Okumura, M., T. Natsume, M.T. Kanemaki, and T. Kiyomitsu. 2018. Dynein-Dynactin-NuMA clusters generate
468 cortical spindle-pulling forces as a multi-arm ensemble. *Elife*. 7.
469 Petry, S. 2016. Mechanisms of Mitotic Spindle Assembly. *Annu Rev Biochem*. 85:659-683.
470 Sampath, S.C., R. Ohi, O. Leismann, A. Salic, A. Pozniakovski, and H. Funabiki. 2004. The chromosomal
471 passenger complex is required for chromatin-induced microtubule stabilization and spindle assembly. *Cell*.
472 118:187-202.
473 Sikirzhytski, V., F. Renda, I. Tikhonenko, V. Magidson, B.F. McEwen, and A. Khodjakov. 2018. Microtubules
474 assemble near most kinetochores during early prometaphase in human cells. *J Cell Biol*. 217:2647-2659.
475 Sillje, H.H., S. Nagel, R. Korner, and E.A. Nigg. 2006. HURP is a Ran-importin beta-regulated protein that
476 stabilizes kinetochore microtubules in the vicinity of chromosomes. *Curr Biol*. 16:731-742.
477 Song, L., A. Craney, and M. Rape. 2014. Microtubule-dependent regulation of mitotic protein degradation. *Mol Cell*.
478 53:179-192.
479 Song, L., and M. Rape. 2010. Regulated degradation of spindle assembly factors by the anaphase-promoting
480 complex. *Mol Cell*. 38:369-382.
481 Uehara, R., and G. Goshima. 2010. Functional central spindle assembly requires de novo microtubule generation in
482 the interchromosomal region during anaphase. *J Cell Biol*. 191:259-267.
483 Walczak, C.E., and R. Heald. 2008. Mechanisms of mitotic spindle assembly and function. *Int Rev Cytol*. 265:111-
484 158.
485 Wiese, C., A. Wilde, M.S. Moore, S.A. Adam, A. Merdes, and Y. Zheng. 2001. Role of importin-beta in coupling
486 Ran to downstream targets in microtubule assembly. *Science*. 291:653-656.
487 Zachariae, U., and H. Grubmuller. 2008. Importin-beta: structural and dynamic determinants of a molecular spring.
488 *Structure*. 16:906-915.
489 Zierhut, C., and H. Funabiki. 2015. Nucleosome functions in spindle assembly and nuclear envelope formation.
490 *Bioessays*. 37:1074-1085.
491

Figure 1

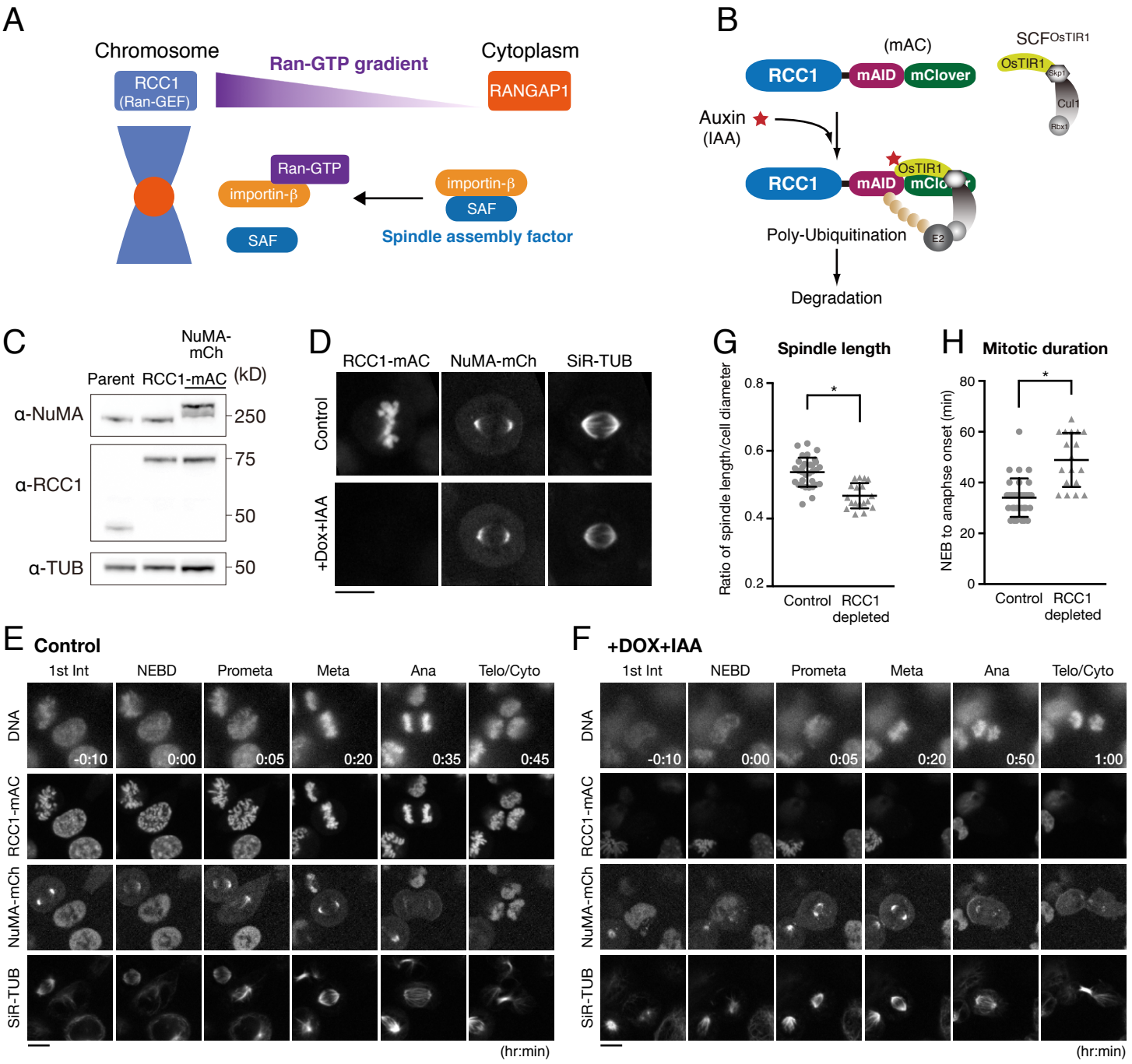

Figure 1. Auxin-inducible degaradation of RCC1 causes short metaphase spindle.

(A) Representation of the mitotic spindle assembly regulated by Ran-related factors. (B) Schematic of the auxin-inducible degradation (AID) system. (C) Immunoblotting for anti-NuMA, anti-RCC1 and anti-α-tubulin (TUB, loading control) showing bi-allelic insertion of the indicated tags. (D) Metaphase RCC1-mAC cells showing live fluorescent images of RCC1-mAC, NuMA-mCherry (mCh), and SiR-tubulin (SiR-TUB) following 24 hrs of Dox and IAA treatment. (E, F) Live fluorescent images of DNA (Hoechst 33342 staining), RCC1-mAC, NuMA-mCh, and SiR-TUB in control (E) and RCC1-depleted (F) cells. (G) Scatterplots of the ratio of spindle length and cell diameter in control (0.54 ± 0.04, n=32) and RCC1-depleted (0.47 ± 0.04, n=23) cells. (H) Scatterplots of mitotic duration (NEBD to anaphase onset) in control (34.1 ± 7.6, n=32) and RCC1-depleted cells (47.2 ± 10.5, n=27). Bars in (G) and (H) indicate mean ± SD from >3 independent experiments. * indicates statistical significance according to Welch's t-test ($p<0.0001$) in (G) and (H). Scale bars = 10 µm.

Figure 2

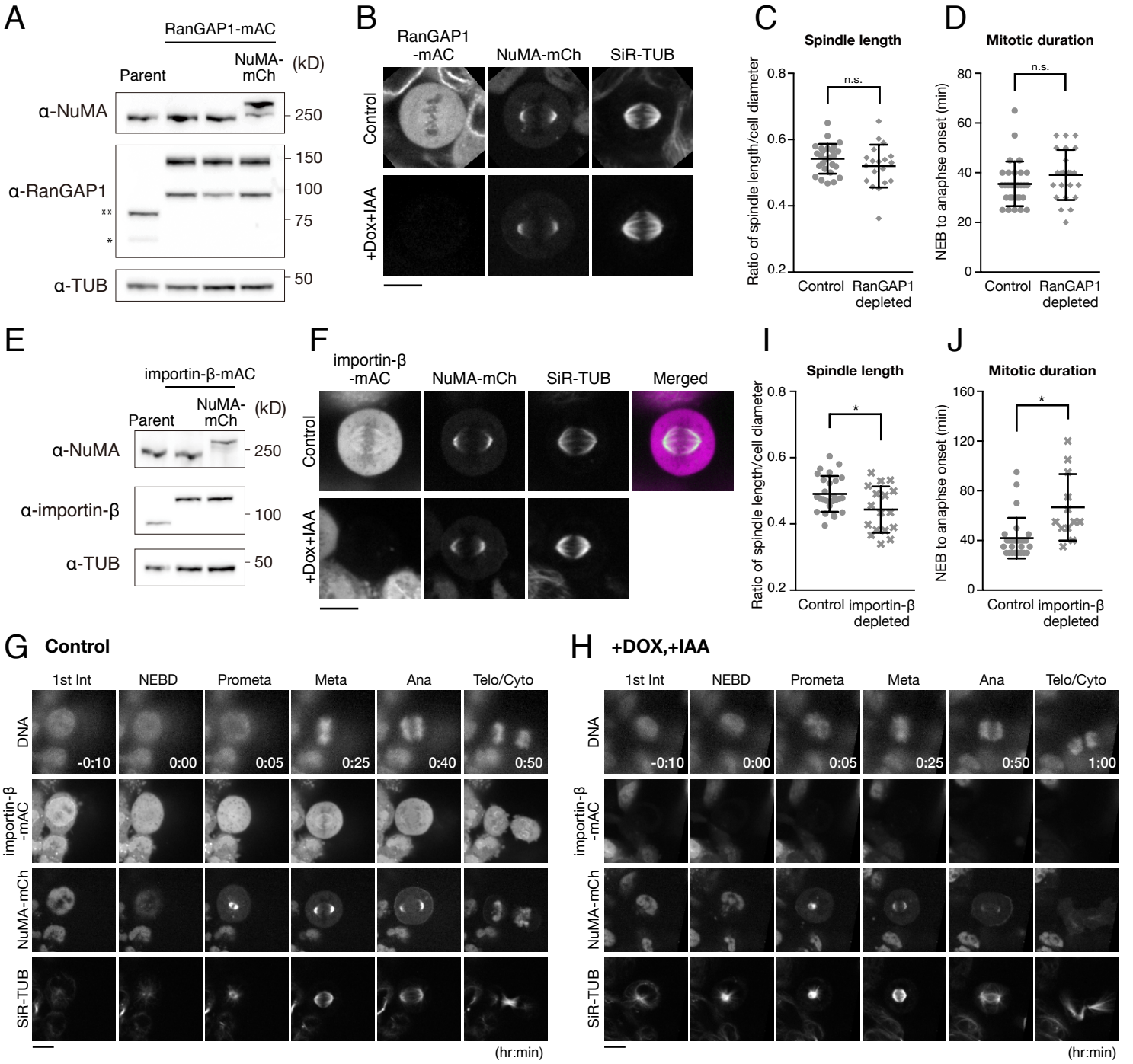

Figure 2. Depletion phenotypes of importin-β are similar to those of RCC1 but not RanGAP1.

(A) Immunoblotting for anti-NuMA, anti-RanGAP1 and anti-α-tubulin (TUB, loading control) showing bi-allelic insertion of the indicated tags. * and ** indicate RanGAP1 and SUMO-1 conjugated RanGAP1, respectively. (B) Metaphase RanGAP1-mAC cells showing live fluorescent images of RanGAP1-mAC, NuMA-mCherry (mCh), and SiR-tubulin (SiR-TUB) after 24 hrs following treatment with Dox and IAA. (C) Scatterplots of the ratio of spindle length and cell diameter in control (0.54 ± 0.04, n=26) and RanGAP1-depleted (0.52 ± 0.07, n=19) cells. (D) Scatterplots of mitotic duration (NEBD to anaphase onset) in control (35.5 ± 9.0, n=29) and RanGAP1-depleted (39.1 ± 10.1, n=23) cells. Bars in (C) and (D) indicate mean ± SD from >3 independent experiments. The differences were not statistically significant based on Welch's t-test in C (p=0.2108) and D (p=0.1851). (E) Western blot detection using anti-NuMA, anti-importin-β and anti-α-tubulin antibodies (TUB, loading control) showing bi-allelic insertion of the indicated tags. (F) Metaphase importin-β-mAC cells showing live fluorescent images of importin-β-mAC, NuMA-mCherry (mCh), and SiR-tubulin (SiR-TUB) following 24 hrs of Dox and IAA treatment. (G, H) Live fluorescent images of DNA (Hoechst 33342 staining), importin-β-mAC, NuMA-mCh, and SiR-TUB in control (G) and importin-β-depleted (H) cells. (I) Scatterplots of the ratio of spindle length and cell diameter in control (0.49 ± 0,05, n=26) and importin-β-depleted (0.44 ± 0.07, n=17) cells. (J) Scatterplots of mitotic duration (NEBD to anaphase onset) in control (41.9 ± 16.3, n=27) and importin-β-depleted (66.7 ± 26.7, n=12) cells. Bars in (G) and (H) indicate mean ± SD from >3 independent experiments. * indicates statistical significance according to Welch's t-test (p<0.05) in (I) and (J). Scale bars = 10 μm.

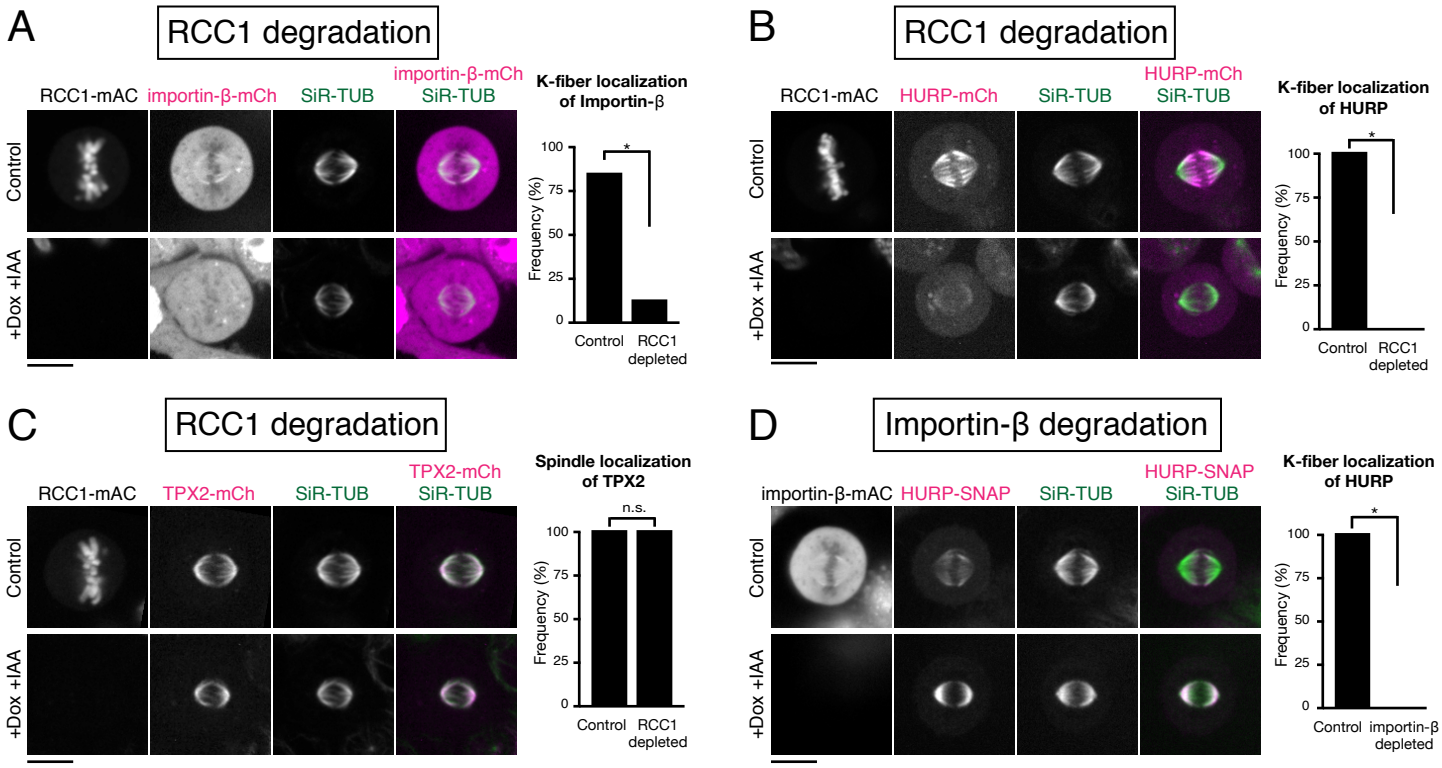

Figure 3. RCC1 and importin-β are required for HURP localization to k-fibers.

(A-C) Left: Metaphase RCC1-mAC cells showing live fluorescent images of RCC1-mAC, SiR-TUB and importin-β-mCherry (mCh) (A), HURP-mCh (B) and TPX2-mCh (C) after 24 hrs following treatment with Dox and IAA. Right: Quantification of k-fiber or spindle localization of importin-β, HURP, or TPX2 in control (n>40) and RCC1-depleted (n>40) cells from 3 independent experiments. (D) Left: metaphase importin-β-mAC cells showing live fluorescent images of importin-β-mAC, HURP-SNAP and SiR-TUB after 24 hrs following treatment with Dox and IAA. Right: quantification of k-fiber localization of HURP in control (n=49) and importin-β-depleted (n=43) cells from 3 independent experiments. * indicates statistical significance according to Z-test (99.9% confidence interval) in (A), (B) and (D). Scale bars = 10 µm.

Figure 4

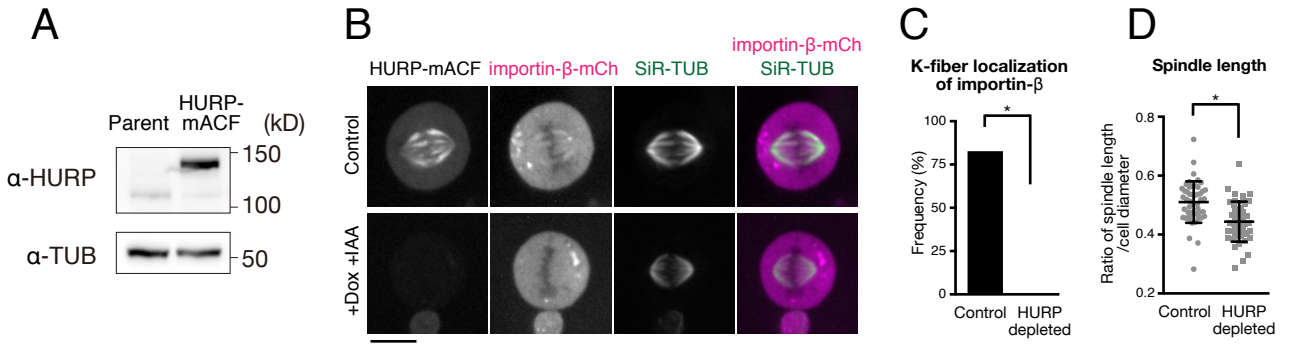

Figure 4. HURP is required to target importin-β to k-fibers and control proper metaphase spindle length.

(A) Immunoblotting for anti-HURP and anti-α-tubulin (TUB, loading control) showing bi-allelic insertion of the indicated tags. (B) Metaphase HURP-mACF cell lines showing live fluorescent images of HURP-mACF, importin-β-mCh and SiR-TUB after 24 hrs following Dox and IAA treatment. (C) Quantification of k-fiber localization of importin-β in control (n=49) and HURP-depleted (n=46) cells from 3 independent experiments. * indicates statistical significance according to Z-test (99.9% confidence interval). (D) Scatterplots of the ratio of spindle length and cell diameter in control (0.64 ± 0.05, n=49) and HURP-depleted (0.52 ± 0.06, n=43) cells. * indicates statistical significance according to Welch's t-test ($p<0.0001$). Scale bars = 10 µm.

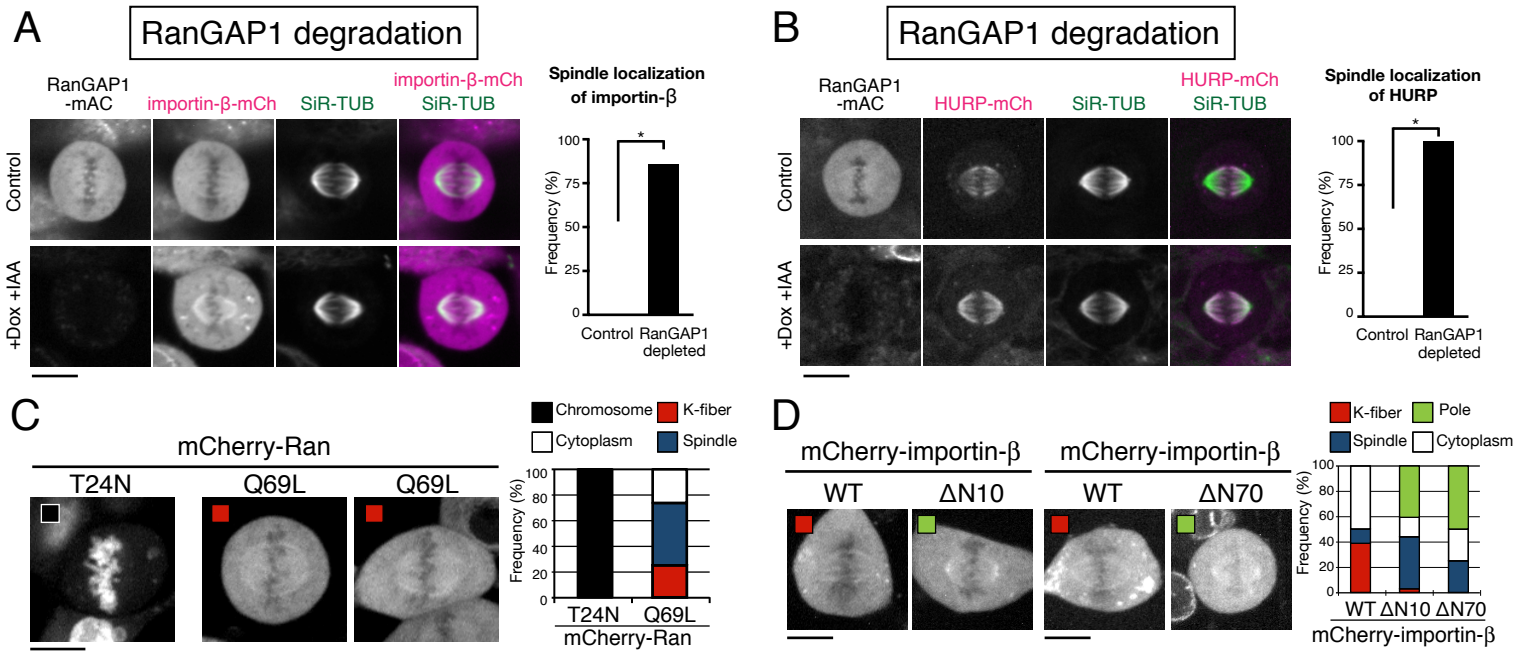

Figure 5. Ran-GTP binding to importin-β is required for k-fiber localization of importin-β

(A, B) Left: metaphase RanGAP1-mAC cells showing live fluorescent images of RanGAP1-mAC, SiR-TUB and importin-β-mCh (A) or HURP-mCh (B) after 24 hrs following Dox and IAA treatment. Right: quantification of k-fiber localization of importin-β or HURP in control (n=45) and RanGAP1-depleted (n>45) cells from 3 independent experiments. * indicates statistical significance according to Z-test (99.9% confidence interval). (C) Left: metaphase HEK293 cells expressing the mCherry-Ran mutants, T24N or Q69L. Right: quantification of mitotic localization of RanT24N (n=30) and RanQ69L (n=45). Maximally projected images from 5 z-sections are shown. (D) Left: metaphase HEK293 cells expressing mCherry-importin-β WT or the mutants, ΔN10 and ΔN70. Right: quantification of mitotic localization of importin-β WT (n=62), ΔN10 (n=32) and ΔN70 (n=16). Maximally projected images from five or three z-sections are shown in the 1st and 2nd panels or in the 3rd and 4th panels, respectively. Scale bars = 10 μm.

Figure 6

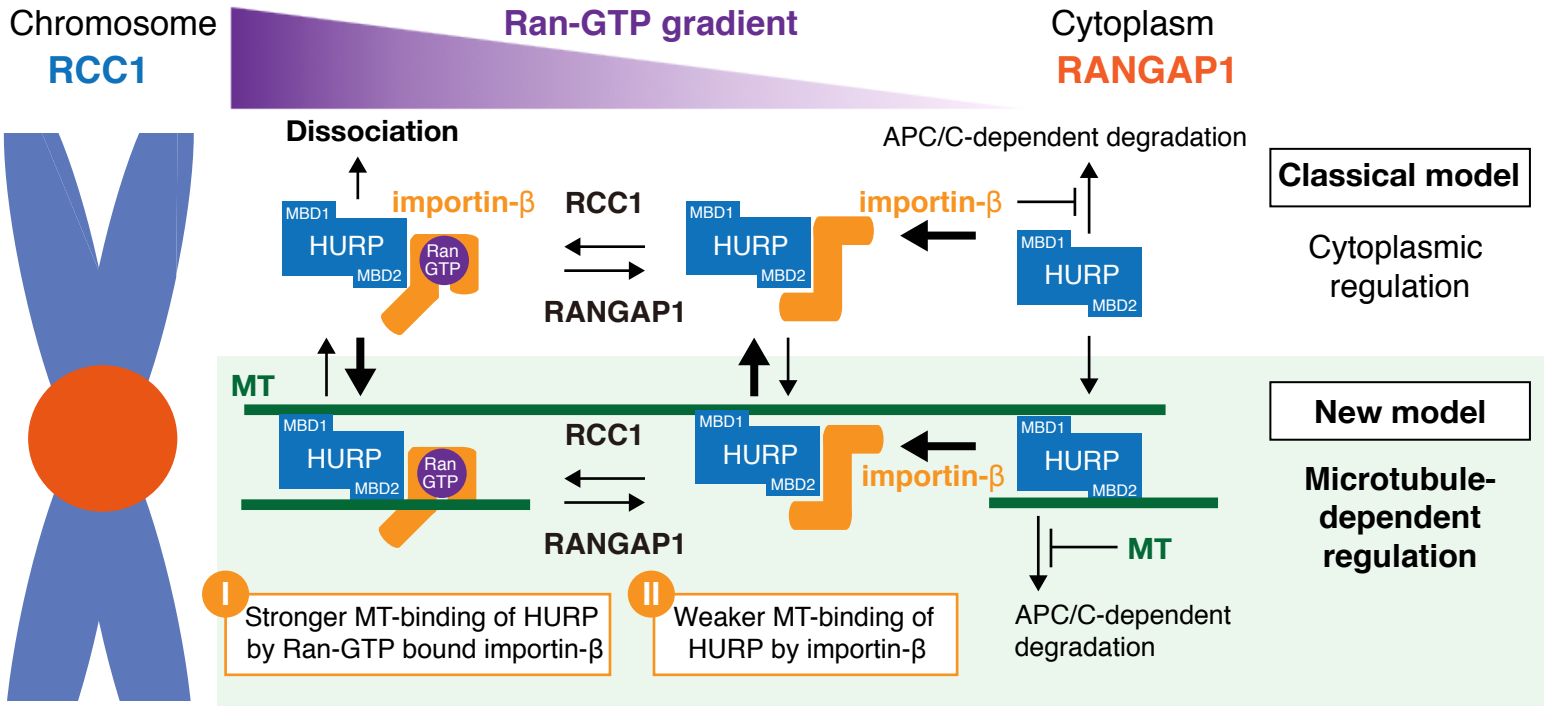

Figure 6. Proposed models of Ran-GTP based regulation of HURP-importin-β complexes

According to the classical model, in the cytoplasm, Ran-GTP binding to importin-β dissociates HURP from importin-β, as described previously (Sillje et al., 2006). In the proposed New Model, in the presence of microtubules, Ran-GTP binding to HURP-importin-β complexes induces a conformational change in importin-β and the ternary complexes would interact more strongly with the microtubules via both MBD1 and MBD2 domains of HURP (New model-I). On spindle microtubules around the spindle pole, Ran-GTP is hydrolyzed by cytoplasmic RanGAP1, and importin-β binding to HURP masks the MBD2 domain, resulting in reduced microtubule affinity of HURP (New model-II). Thus, the dual functions of importin-β in response to Ran-GTP gradient achieve k-fiber accumulation of HURP near the chromosomes. Both importin-β and microtubule act as a protector of HURP from APC/C-dependent degradation by masking the APC/C recognition motif in the MBD2 of HURP (Song et al., 2014).

Supplemental Figure S1

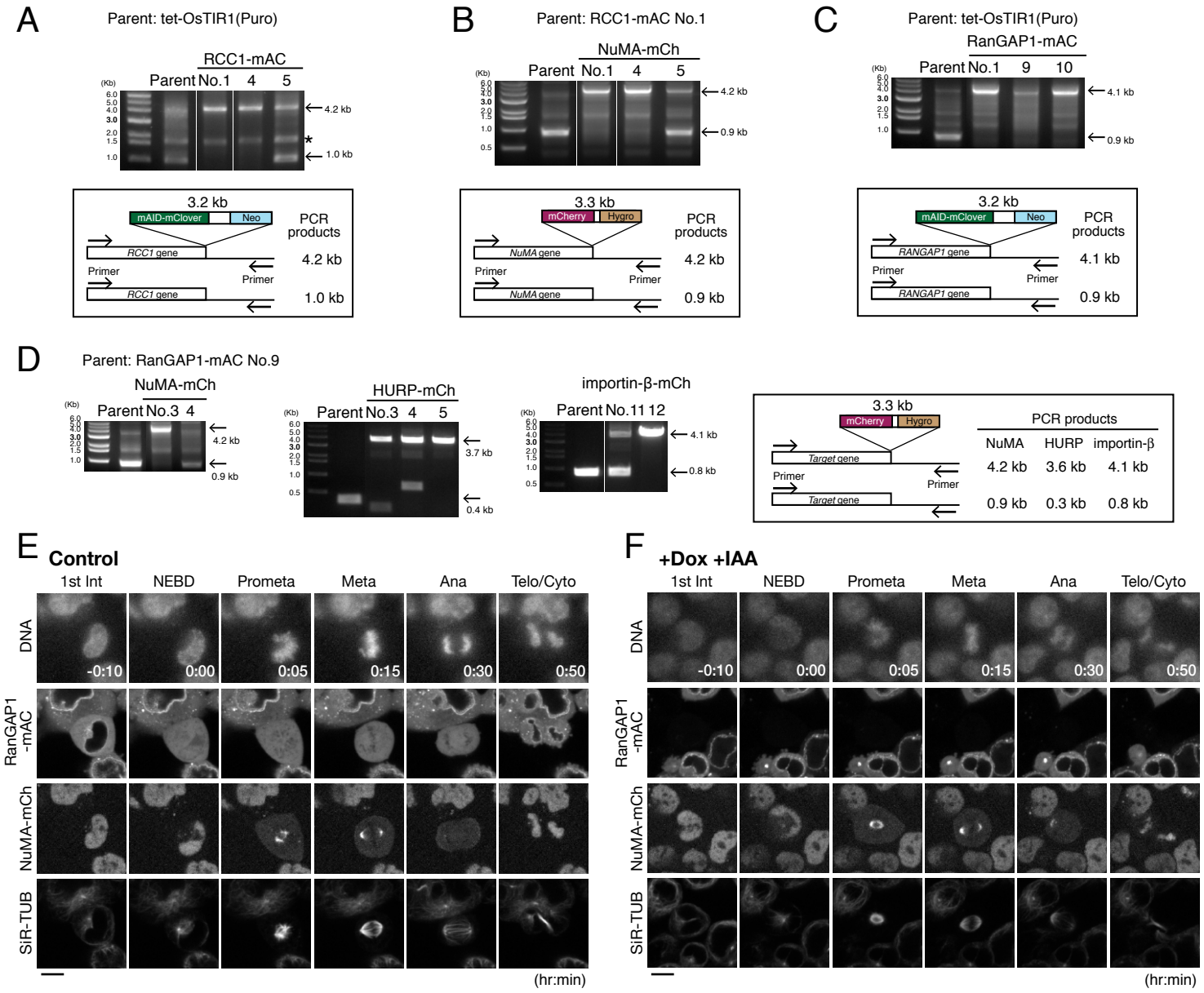

Figure S1. Generation of cell lines for auxin-inducible degaradation of endogenous RCC1 and RanGAP1

(A) Genomic PCR showing clone genotypes after neomycin (Neo) selection. Clone No.1 was used as a parental cell in the second selections. * indicates a non-specific band. (B) Genomic PCR showing clone genotypes after hygromycin (Hygro) selection. Clone No.1 was used in this study. (C) Genomic PCR showing clone genotypes after neomycin (Neo) selection. The clone No.9 was used as a parental cell in the second selections. (D) Genomic PCR showing clone genotypes after hygromycin (Hygro) selection. The clones No.3 (NuMA-mCh), No.5 (HURP-mCh), and No.12 (importin-β-mCh) were used, respectively. (E, F) Live fluorescent images of DNA (Hoechst 33342 staining), RanGAP1-mAC, NuMA-mCh, and SiR-TUB in control (E) and RanGAP1-depleted (F) cells. Scale bars = 10 µm.

Supplemental Figure S2

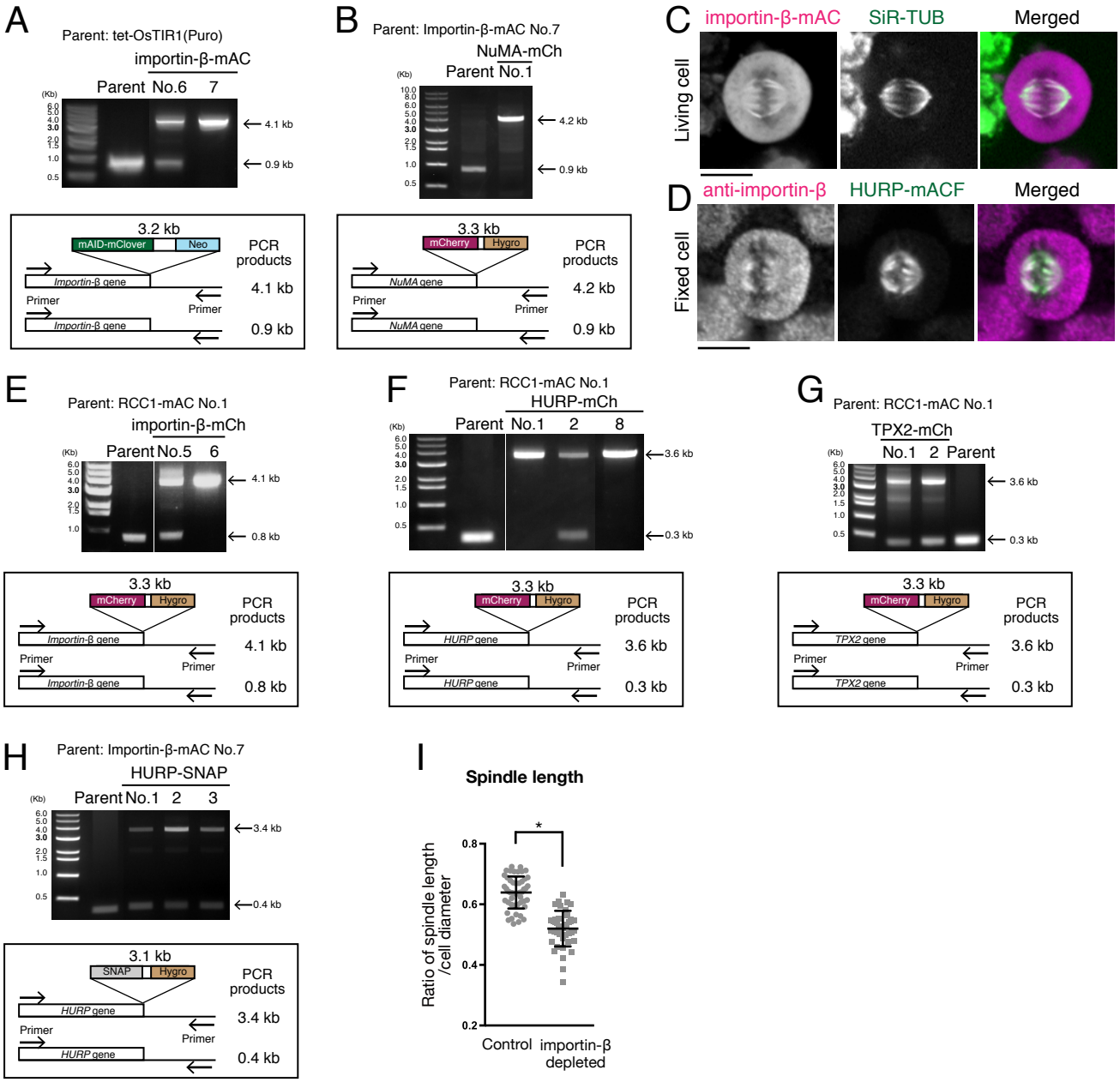

Figure S2. Generation of cell lines for auxin-inducible degaradation of endogenous importin-β

(A) Genomic PCR showing clone genotypes after neomycin (Neo) selection. The clone No.7 was used as a parental cell in the second selections. (B) Genomic PCR showing clone genotype after hygromycin (Hygro) selection. Clone No.1 was selected for further use. (C) Metaphase importin-β-mAC cells showing live fluorescent images of importin-β-mAC, and SiR-TUB. Single z-section images are shown. (D) Immunofluorescence images of fixed metaphase cells showing k-fiber localization endogenous importin-β and mAID-tagged HURP (HURP-mACF). The maximally projected images from 3 z-sections are shown. (E-H) Genomic PCRs showing clone genotypes after hygromycin (Hygro) selections. Clones No.6 (E), No. 8 (F), No.1 (G), and No.3 (H) were used. The mCherry or SNAP cassette was inserted into only one copy of TPX2 (G), or HURP (H) gene loci, respectively. (I) Scatterplots of the ratio of spindle length and cell diameter in the cell line expressing importin-β-mAC and HURP-SNAP: control (0.52 ± 0.07, n=49) and importin-β-depleted (0.44 ± 0.07, n=46) cells. * indicates statistical significance according to Welch's t-test ($p<0.0001$).

Supplemental Figure S3

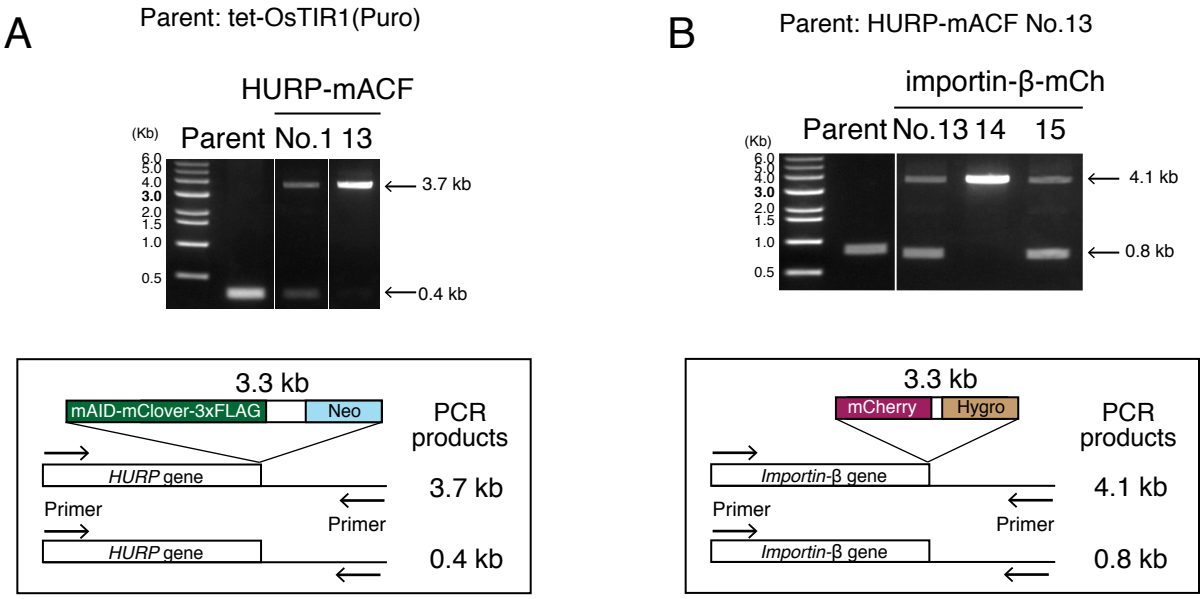

Figure S3. Generation of cell lines for auxin-induced degradation of endogenous HURP

(A) Genomic PCR showing clone genotype after neomycin (Neo) selection. Clone No.13 was used as a parental cell in the second selections. (B) Genomic PCR showing clone genotypes after hygromycin (Hygro) selection. Clone No.14 was used.

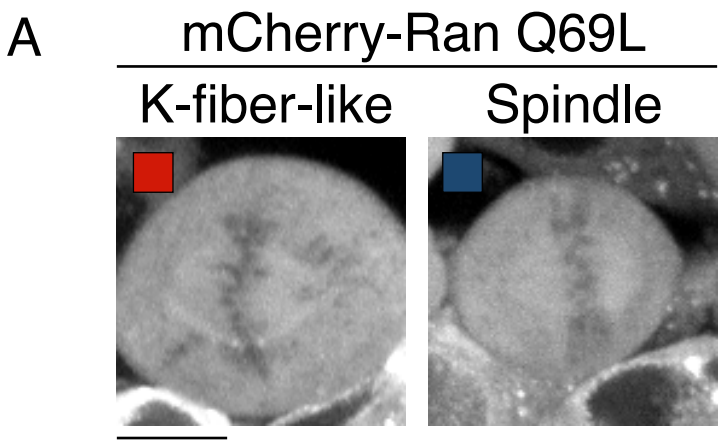

Figure S4. Mitotic localization of RanQ69L mutant

(A) Live fluorescent images of metaphase HEK293 cells transiently expressing the mCherry-RanQ69L mutant. About 25% of cells display k-fiber-like localization. In a few cases, kinetochore-like punctate signals were seen (left). About 50% of cells show spindle-like fuzzy localization (right).